

Winning Strategy for Iron-Based ATRP Using In Situ Generated Iodine as a Regulator

Zhi-Hao Chen, Yang Ma, Xiao-Yan Wang,* Xiu-Li Sun, Jun-Fang Li, Ben-Hu Zhu, and Yong Tang*



Cite This: *ACS Catal.* 2020, 10, 14127–14134



Read Online

ACCESS |



Metrics & More



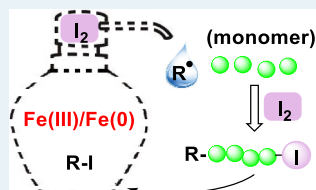
Article Recommendations



Supporting Information

ABSTRACT: Iron-based catalysts for atom-transfer radical polymerization (ATRP) are attractive in the sustainability aspects of green polymer chemistry but usually exhibit lower efficiency and controllability over the polymerization, as well as poorer tolerance to polar groups, compared to copper catalysts. Herein, β -ketamine/iron complexes, combining a strategy employing in situ generated iodine as a regulator, have been developed for improving the efficiency and robustness of iron-catalyzed ATRP. The catalyst system realizes low catalyst loading, ultrahigh molecular weight, robustness over polar groups, efficient polymerization of acrylate, and forthrightly synthesizing block copolymers, which are challengeable for common iron catalysts. A mechanism was proposed based on experimental results, which mainly involves the ATRP activation process by Fe(II) and the I_2 -mediated deactivation process.

KEYWORDS: iron, iodine, catalyst, controlled radical polymerization, mechanism



A Winning Strategy
green catalytic system
5 ppm of catalyst
 M_n up to 303.8 kg/mol
in situ chain extension
efficient for acrylate
robustness over polar group

INTRODUCTION

Following the key reports by Matyjaszewski and Sawamoto in the mid-1990s, atom-transfer radical polymerization (ATRP) has been positioned as an extensively applicable synthetic strategy in various fields.^{1–4} Although several elegant catalysts have been developed for ATRP,^{5,6} there remains a need to develop highly active catalyst systems with low toxicity, especially in the synthesis of materials for biomedical applications. The iron-based ATRP catalysts are particularly attractive in regard to the sustainability aspects in green polymer chemistry because of the natural capacity of the body to store and transport this metal.^{7,8} However, compared to copper catalysts,⁹ iron catalysts generally exhibit lower efficiency and controllability over the polymerization^{10–22} and are more vulnerable to “poison” by polar groups via ligand dissociation or exchange.⁴ Iron catalysts are usually accompanied by some defects, including relatively high catalyst loading (>100 ppm),^{23–25} limited applicable monomers and solvents,^{26–28} restricted molecular weight (MW) (<100 kg/mol), low efficiency for acrylate polymerization,²⁹ and difficulty in forthrightly synthesizing block copolymers through in situ chain expansion.^{5,30,31} Based on in situ (re)generation of the activator species, the recently developed ATRP techniques can only partially solve the above problems. For example, the photoinduced Fe-catalyzed ATRP realized the block copolymerization via in situ chain extension with different monomers.^{32–34}

The key factor for the controllability of ATRP is to achieve a low and constant radical concentration. As iodine is an excellent alkyl radical scavenger via a reversible process (eq 1),^{35–42} we envisioned that I_2 could act as a potential regulator

to control the radical concentration for iron-based ATRP. Based on this strategy, we found that side-armed^{8,43–48} β -ketamine ligands/iron is an excellent catalytic system for ATRP, which can deal with all the aforementioned issues associated with iron catalysts. Herein, we will report the preliminary results.

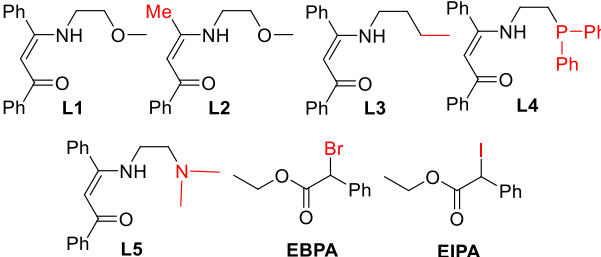


RESULTS AND DISCUSSION

Polymerization of MMA Regulated by I_2 . Initially, the polymerization of MMA was carried out for 10 h at 30 °C in THF employing **L1**/FeBr₃/Fe(0) as the catalytic system. Three commonly employed alkyl bromides were utilized as the initiators (Table S1), including ethyl α -bromoisobutyrate, ethyl α -bromophenylacetate (EBPA), and 2-bromopropionitrile. Not surprisingly, the resultant polymers exhibit broad MW distributions ($\mathcal{D}s = 1.7$ –2.2), indicating the poor controllability of the polymerizations (runs 1–3). Based on the strategy mentioned above, the polymerization of MMA was conducted using EBPA as the initiator with the addition of I_2 (Table 1). The \mathcal{D} value initially narrows with the increase of I_2 dosage and levels off when the $n(I_2)/n(\text{EBPA})$ reaches 0.375 (runs 2–4). When this ratio reaches 1.0, the polymerization

Received: October 4, 2020

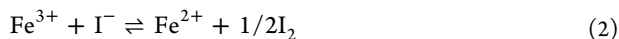
Revised: November 5, 2020

Table 1. Polymerization of MMA Regulated by I_2^a


| run | ligand | initiator | $n(I_2)/n(EXPA)$ | conv. ^b (%) | $M_{n,GPC}$ ($M_{n,theo}$) (kg/mol) | \mathcal{D} |
|-----|--------|-----------|------------------|------------------------|---|---------------|
| 1 | L1 | EBPA | | 87 | 10.3 (8.9) | 1.63 |
| 2 | L1 | EBPA | 0.125 | 87 | 11.4 (9.0) | 1.52 |
| 3 | L1 | EBPA | 0.375 | 84 | 10.0 (8.7) | 1.28 |
| 4 | L1 | EBPA | 0.625 | 86 | 10.7 (8.9) | 1.29 |
| 5 | L1 | EBPA | 1.000 | 43 | 4.5 (4.6) | 1.14 |
| 6 | L1 | EIPA | | 85 | 11.6 (8.8) | 1.27 |
| 7 | L1 | EIPA | 0.125 | 82 | 12.2 (8.5) | 1.22 |
| 8 | L1 | EIPA | 0.250 | 83 | 11.2 (8.6) | 1.25 |
| 9 | L1 | EIPA | 0.375 | 81 | 12.8 (8.4) | 1.25 |
| 10 | L1 | EIPA | 0.500 | 59 | 7.0 (6.2) | 1.14 |
| 11 | L2 | EIPA | | 71 | 32.8 (7.4) | 1.51 |
| 12 | L3 | EIPA | | 57 | 50.2 (6.0) | 1.70 |
| 13 | L4 | EIPA | | 74 | 25.5 (7.7) | 1.78 |
| 14 | L5 | EIPA | | 0 | | |

^aConditions: $n(MMA):n(Initiator):n(FeBr_3):n(Ligand):n(Fe(0)) = 100:1:0.5:0.75:2$, THF was used as a solvent (50% V_{total}), 30 °C, and 10 h. ^bMonomer conversion measured by 1H NMR.

rate decreases significantly. These results verify the feasibility of our strategy and indicate that I_2 acts as an efficient deactivator (regulator of radical concentration), but excessive I_2 will hinder the polymerization (run 5).



The oxidation of iodide ion (I^-) to I_2 by Fe(III) is a well-known redox reaction that conforms to the redox potential and Gibbs free energy (eq 2, more discussions on this below).^{49,50} Considering that I_2 could generate in the presence of I^- and Fe(III), we subsequently applied α -iodophenylacetate (EIPA) instead of EBPA as the initiator without the addition of I_2 to simplify our strategy (run 6). A narrowed MW distribution is achieved with high MMA conversion of 85% ($\mathcal{D} = 1.27$).^{51,52} The polymerization using EIPA as the initiator is well controlled without the detection of induction period, which is indicated by the linear first-order kinetic plot across the zero point and the gradual increase of MW with the conversion as well as the throughout narrow MW distributions ($\mathcal{D} \approx 1.2$) (Table S2 and Figure S1). Using EIPA as the initiator, the addition of I_2 has little influence on the control over MW, indicating that in situ generated I_2 via the oxidation of I^- with Fe(III) species is sufficient as a regulator (runs 7–9). When the equivalent ratio of I_2 /EIPA reaches 0.5 (run 10), the polymerization rate significantly decreases. Furthermore, we monitored the reactions of I_2 /EBPA (0.375 equiv, run 3) and I_2 /EIPA (0.375 equiv, run 9) systems. The reaction process and the polymerization results are very similar. As shown in Figure 1, from the very beginning of the reaction, the polymerizations are very controllable (Tables S3 and S4). These results suggest that the different initiators (EBPA or

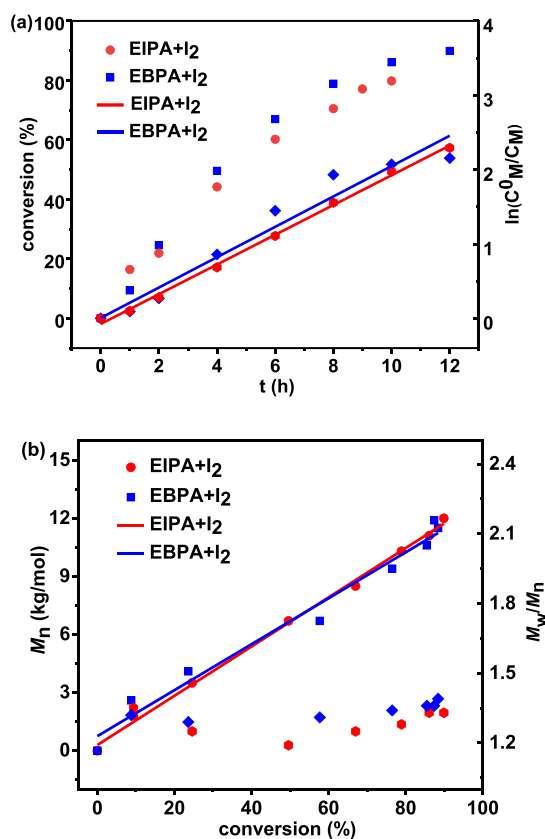


Figure 1. (a) First-order kinetic plot and (b) evolution of M_n and \mathcal{D} (M_w/M_n) as a function of conversion for the ATRPs of MMA with the addition of I_2 (runs 3 and 9 in Table 1).

EIPA) have little effect on the controllability of polymerization in the presence of I_2 .

Ligand Effects. We next investigated the ligand effects under the same conditions. As shown in runs 11–14, the ligand scaffolds have slight influence on either the monomer conversion or controllability (L2 vs L1). By contrast, the side arm of the ligand obviously affects the polymerization. The ligand without coordination side arm (L3) gives much lower conversion (57%) and much poorer controllability ($\mathcal{D} = 1.70$). The catalyst lacking donor arm might be more easily coordinated by solvent (THF), and the generated crowded catalytic environment is detrimental to the process of atom transfer. Similarly, in this case, one metal center might be chelated with two or more ligands in the reaction system, which will also lead to a crowded environment around the catalytic center. When the methoxy is changed into a diphenylphosphine group (L4), the monomer conversion declines to 74%, and the MW distribution is widened to 1.78. Notably, the polymerization is completely inhibited when the methoxy group is altered to a dimethylamine group (L5). This might be due to the fact that the strong coordination of side arm reduces the halidophilicity of the Fe(III) complex, thus inhibiting the activation process.

Low Catalyst Loading, Ultrahigh MW, and Excellent Tolerance toward Polar Group. Using EIPA and L1, similar polymerization rate and controllability of MW are obtained when the catalyst dosage decreased from 5000 ppm (Table 1, run 6) to 50 ppm (Table 2, run 1). Further reducing the catalyst loading to 5 ppm, a high conversion of 81% is obtained by doubling the reaction time (19 h) and the polymerization is

Table 2. Polymerizations of Various Monomers under Different Conditions^a

| run | monomer | initiator | sol. | DP _{target} | FeBr ₃ /M ^b (ppm) | t (h) | conv. ^c (%) | M _{n,GPC} (M _{n,theo}) (kg/mol) | Đ |
|-------------------|---------|-----------|---------|----------------------|---|-------|------------------------|--|------|
| 1 | MMA | EIPA | THF | 100 | 50 | 10 | 84 | 12.8 (8.7) | 1.25 |
| 2 | MMA | EIPA | THF | 100 | 5 | 19 | 81 | 11.7 (8.4) | 1.22 |
| 3 | MMA | EBPA | THF | 100 | 5 | 19 | 71 | 51.4 (8.0) | 2.01 |
| 4 ^d | MMA | EBPA | THF | 100 | 5 | 19 | 79 | 10.3 (8.2) | 1.33 |
| 5 ^e | MMA | EIPA | THF | 1000 | 5 | 24 | 84 | 97.7 (84.4) | 1.50 |
| 6 ^e | MMA | EIPA | THF | 5000 | 5 | 82 | 59 | 303.8 (295.6) | 1.53 |
| 7 | MMA | EIPA | MeOH | 100 | 5000 | 10 | 82 | 10.4 (8.2) | 1.33 |
| 8 | MMA | EBPA | MeOH | 100 | 5000 | 10 | 99 | 37.5 (9.9) | 2.12 |
| 9 ^d | MMA | EBPA | MeOH | 100 | 5000 | 10 | 77 | 15.0 (8.0) | 1.64 |
| 10 | MMA | EIPA | DMF | 100 | 5000 | 10 | 91 | 12.4 (9.1) | 1.35 |
| 11 ^f | MMA/MAA | EIPA | THF | 100 | 4444 | 21 | 56/52 | 3.2 (6.4) | 1.38 |
| 12 | PEGMA | EIPA | THF | 25 | 20000 | 10 | >99 | 12.0 (12.7) | 1.16 |
| 13 | St | EIPA | THF | 100 | 5000 | 48 | 40 | 3.1 (4.2) | 1.37 |
| 14 ^e | St | EIPA | THF | 100 | 125 | 48 | 76 | 9.4 (7.9) | 1.21 |
| 15 ^g | MA | EIPA | DMF | 200 | 12.5 | 12 | 75 | 53.8 (13.2) | 1.53 |
| 16 ^{g,h} | MMA/MA | EIPA | THF | 100 | 25 | 17 | 92/75 | 11.4 (11.5) | 1.45 |
| 17 ^{g,i} | MMA/MA | EIPA | THF/DMF | 100 | 25 | 10 | 93/65 | 25.0 (15.2) | 1.54 |

^aReaction conditions: $n(\text{monomer}):n(\text{EIPA}):n(\text{Fe(0)}) = \text{DP}_{\text{target}}:1:2$, $n(\text{L1}):n(\text{FeBr}_3) = 1.5:1$, 30 °C, and $V_{\text{solvent}} = 50\% V_{\text{total}}$. ^bFeBr₃ loading relative to the monomer. ^cMonomer conversion measured by ¹H NMR. ^dWith the addition of I₂ (0.375 equivalent). ^e60 °C. ^f $n(\text{MMA}):n(\text{MAA}) = 89:11$. ^g60 °C. ^h $n(\text{EIPA}):n(\text{I}_2) = 1:0.13$. ⁱ $n(\text{MMA}):n(\text{MA}) = 5:1$. ^j $n(\text{MMA}):n(\text{MA}) = 1:1$, $V(\text{THF})/V(\text{DMF}) = 2/1$.

still well controlled (run 2). Subsequently, we targeted high degrees of polymerization (DP) of 1000 and 5000 (runs 5–6), achieving high MWs of 97.7 and 303.8 kg/mol, respectively, as well as acceptable MW distributions ($\bar{D} = \sim 1.5$). Notably, our catalytic system exhibits high robustness over the polar group in monomers and solvents. The MMA polymerizations proceed successfully in polar solvents (runs 7 and 10), including MeOH and DMF achieving high conversions of 82 and 91% in 10 h, respectively, with MWs close to theoretical values and narrow MW distributions ($\bar{D} = \sim 1.3$). By contrast, the control of the polymerization is very poor when employing EBPA as the initiator with 5 ppm of catalyst (run 3) or using MeOH as a solvent (run 8). The corresponding polymerization reactions with the addition of I₂ (0.375 equiv) were also conducted. The much more controlled MWs again suggest that iodine plays a role in regulating polymerization when employing low catalyst loading (run 4 vs run 3) or using a polar solvent (run 9 vs run 8).

Besides, functional methacrylate monomers, including poly(ethylene glycol) methacrylate (PEGMA) and methacrylic acid (MAA), can be polymerized under conditions of homopolymerization or copolymerization (runs 11–12). The narrow MW distributions demonstrate the excellent controllability of the polymerizations. In addition, this system is suitable for styrene polymerizations, which are well controlled with narrow MW distributions and MWs close to theoretical values even at room temperature (runs 13–14).

Polymerization of Methyl Acrylate. The iron-based ATRP of acrylates has been challenging and less efficient, often leading to low monomer conversions, low initiation efficiency, and polymers with high dispersities.²⁹ Acrylate-based secondary radicals are more susceptible to form organometallic species with the Fe(II) activators than the tertiary methacrylate-based radicals, resulting in the high degree of catalytic radical termination or catalytic chain transfer reactions. Moreover, the lower activity of the dormant acrylate chain end may also contribute to the lower efficiency of the iron-based ATRP of acrylates. Based on our strategy, we also anticipated to conquer this challenge with our catalytic system.

The polymerizations of methyl acrylate (MA) were conducted at 60 °C in DMF to enhance the activity of dormant acrylate chain end. In order to suppress the formation of organometallic species and improve the controllability of the polymerization, a very low amount of catalyst (12.5 ppm) was employed with the addition of I₂ (0.13 equivalent of EIPA). As shown in Table 2, the homopolymerization of MA with a DP_{target} of 200 (run 15) achieves a MA conversion of 75% in 12 h and a \bar{D} value of 1.53. Furthermore, the copolymerizations of MMA and MA with $n(\text{MMA})/n(\text{MA}) = 5/1$ or $1/1$ proceed efficiently, with MA conversions of 65–75% (runs 16–17) and \bar{D} values of ~ 1.5 . Research about the highly efficient iron-based ATRP of MA is under way.

“Livingness” of the Resultant Polymer. We carried out elemental analysis to determine the iodine content of the polymer obtained using 500 ppm of FeBr₃ catalyst ($n_0(\text{I})/n_0(\text{Br}) = 40/3$). The result (Table S5) shows that the polymer produced at 80% conversion includes 95% of active polymer possessing iodine chain end (with $\pm 5\%$ experimental error). Figure S2 shows the ¹H NMR spectrum of PMMA ($M_{n,\text{GPC}} = 7.3$ kg/mol). According to the literature⁵³ as well as ¹³C and two-dimensional NMR spectra analysis (Figures S3 and S4), the main peak and its shoulder peak at 3.57–3.68 ppm are assigned to the monomer units (methoxycarbonyl a) in the middle of the chain, while the downfield-shifted peak at 3.73–3.78 ppm is assigned to the ω -terminal chain end unit (methoxycarbonyl a') adjacent to iodine. From the peak area of a', $M_{n,\text{NMR}}$ is calculated as 7298 kg/mol, and the fraction of the halogen chain end ($M_{n,\text{GPC}}/M_{n,\text{NMR}}$) is 100%.⁵⁴

Taking advantage of this high chain end fidelity, we prepared block copolymers by in situ chain extensions after the nearly complete monomer conversion of the first block using 50 ppm of catalyst. With a second aliquot of MMA, the polymerization produces higher MW polymer ($M_n = 13.7$ kg/mol), obtaining a final dispersity of 1.39, with the conversions of 92 and 74%, respectively, for the first and second block (Figure 2a and Table S6). The chain of a PMMA macroinitiator is also in situ extended employing butyl methacrylate (BMA) as the second monomer, yielding a well-defined poly(MMA-*b*-BMA) diblock

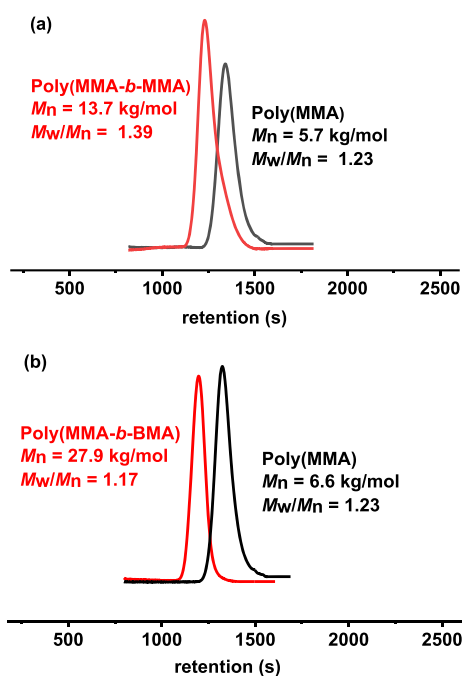
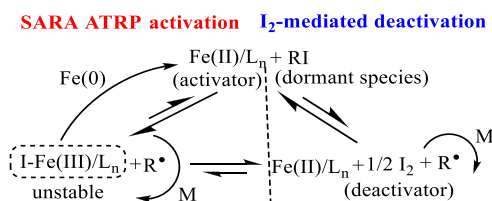


Figure 2. GPC traces of (a) in situ chain extension of poly(MMA-*b*-MMA) (Table S6) and (b) in situ block copolymerization of poly(MMA-*b*-BMA) (Table S7).

copolymer with a final dispersity of 1.17 (Figure 2b and Table S7), with the conversions of 96 and 70%, respectively, for the first and second block.

Plausible Mechanism. We proposed a mechanism for iron-mediated ATRP using iodinated initiator, which mainly involves the ATRP activation process by Fe(II) and the I_2 -mediated deactivation process (Scheme 1). According to the

Scheme 1. Proposed Mechanism for Iron-Mediated Controlled Radical Polymerization Using the Iodinated Initiator



redox sequence, I–Fe(III) is unstable as I^- reduces Fe(III) to Fe(II) (eq 2), which helps avoid the accumulation of the deactivator and maintain sufficient activator concentration. Meanwhile, the in situ generated I_2 acts as an efficient deactivator to trap the radical species. This strategy could ensure the highly efficient activation–deactivation process, thus maintaining constant and low radical concentration. Therefore, the efficiency, controllability, and robustness of the iron-catalyzed ATRP are improved using iodinated initiator instead of commonly used brominated reagent.

SARA ATRP Activation. Without the addition of iron catalyst [L1/FeBr₃/Fe(0)], the polymerizations do not occur within 10 h, even at 80 °C or with irradiation at 365 nm (runs 1–2, Table 3). These control experiments indicate that the polymerization requires the iron catalyst [L/FeBr₃/Fe(0)] to occur. Besides, two radical trap experiments were performed,

Table 3. Control Experiments to Support the SARA ATRP Activation^a

| run | catalyst | T (°C) | conv. ^b (%) |
|----------------|----------------------|------------------|------------------------|
| 1 | | 30 or 80 | 0 |
| 2 ^c | | 30 (irradiation) | 0 |
| 3 ^d | L1/FeBr ₃ | 30 | 0 |
| 4 ^e | L1/Fe(0) | 30 | 3.5 |
| 5 ^f | L1 | 30 | 0 |

^aConditions: $n(\text{MMA}):n(\text{EIPA}) = 100:1$, THF was used as a solvent (50% V_{total}), and 10 h. ^bMonomer conversion measured by ¹H NMR. ^cWith irradiation at 365 nm. ^d $n(\text{MMA}):n(\text{FeBr}_3):n(\text{L1}) = 100:0.5:0.75$. ^e $n(\text{MMA}):n(\text{Fe(0)}):n(\text{L1}) = 100:2:0.75$. ^f $n(\text{MMA}):n(\text{L1}) = 100:0.75$.

in which EIPA and TEMPO (4.0 equiv) were stirred in THF with or without the addition of iron catalyst. The ¹H NMR spectra (Figure S5) show that the signals of EIPA disappear completely within 3 h in the presence of iron catalyst. New signals appear and match those of pure EPA-TEMPO (Scheme S1). In comparison, the signals of the initiator have no change without the addition of iron catalyst. This result further demonstrates that iron catalyst is necessary for the efficient generation of R^* from R–I.

The polymerization using the catalytic system of L/FeBr₃/Fe(0) conforms to the definition of supplemental activator and reducing agent atom-transfer radical polymerization (SARA ATRP),⁹ with a zero-valent metal acting as a supplemental activator to slowly and continuously compensate for the loss of activating species due to the unavoidable radical termination reactions. Besides, under similar conditions, without the addition of Fe(0), the polymerizations do not occur within 10 h using the L1/FeBr₃ catalytic system, excluding that Fe(III) decomposed into Fe(II) and Br[•] to initiate the polymerization (run 3). In the absence of FeBr₃, the conversion of MMA is only 3.5% within 10 h, indicating that single electron transfer makes little contribution to the activation process (run 4). In order to investigate the influence of reversible complexation-mediated polymerization on the polymerization process, only the β -ketamine ligand (L1) was used as the catalyst and the polymerizations do not occur within 10 h (run 5). These results further argue that the polymerizations proceed under SARA ATRP activation and the active species should be an Fe(II) complex.

Generation of I_2 and the Instability of I–Fe(III). Next, we attempted to detect the generation of I_2 using the UV–vis analysis, which is a widely used method to detect iodine.^{55,56} In order to avoid the absorption peak of I_2 being masked by the strong signals of our ligands, the catalyst system was simplified to FeBr₃/Fe(0) or FeBr₂. As shown in Figure S6, the signals of I_2 (around 292 and 368 nm) are detected. Furthermore, TEMPO was added to make the generation of I_2 irreversible, and thus, the signals of I_2 could be observed more clearly (Figure 3a). According to the mechanism shown in Scheme 1, the reaction of EIPA with FeBr₂ (1 equiv) and TEMPO (1.5 equiv) will eventually yield I_2 , FeBr₂, and EPA-TEMPO. After 12 h, three peaks around 234, 292, and 368 nm appear in the UV–vis spectrum of the reaction mixture (Figure 3c, purple line), perfectly matching those of the preconceived three products (I_2 , FeBr₂, and EPA-TEMPO), either an individual one or their mixture.^{55,56} Besides, iodine also contributes to a wide visible light wavelength range extended to about 690 nm. We employed the same method to track the reaction of FeBr₃

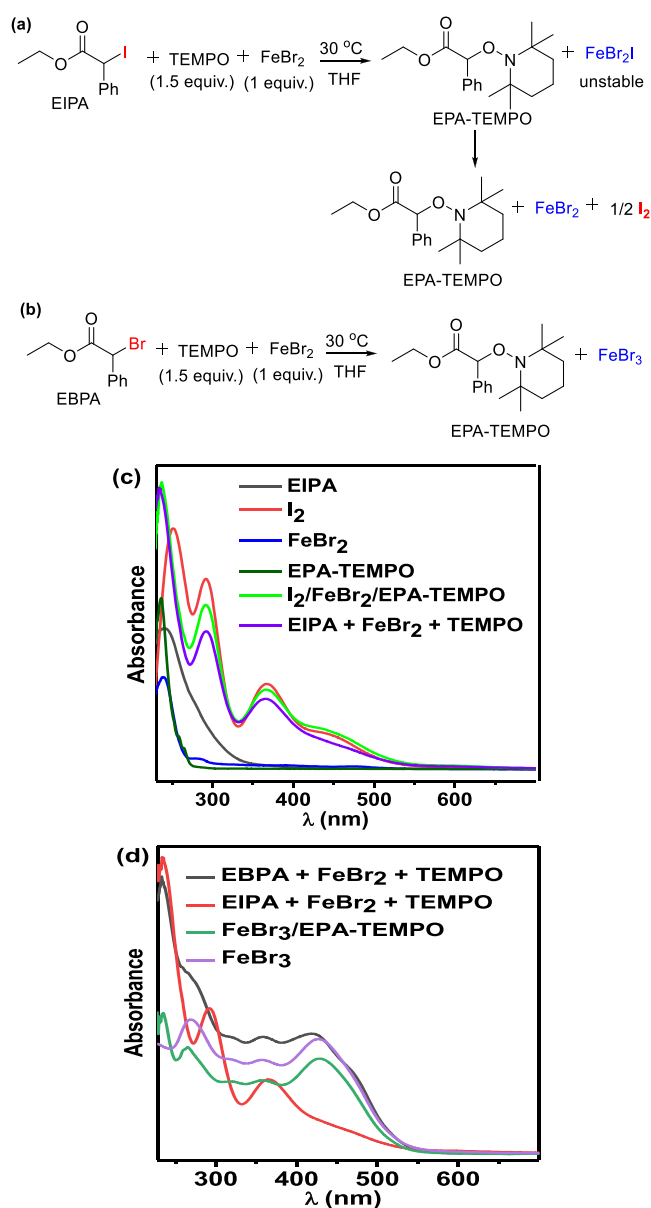


Figure 3. Radical trap experiments of (a) EIPA and (b) EBPA tracked by UV-vis spectra ($[\text{initiator}] = 1.7 \text{ mM}$). (c) UV-vis absorption spectra of I_2 , FeBr_2 , EPA-TEMPO and their mixture ($\text{I}_2/\text{FeBr}_2/\text{EPA-TEMPO}$), EIPA, and the reaction system of EIPA with FeBr_2 and TEMPO (for 12 h) and (d) UV-vis absorption spectra of the reaction system of EBPA with FeBr_2 and TEMPO (for 12 h); the reaction system of EIPA with FeBr_2 and TEMPO (for 12 h); the mixture of $\text{FeBr}_3/\text{EPA-TEMPO}$, as well as pure FeBr_3 . THF was used as the solvent.

with Bu_4NI (1 equiv). After 10 min of the reaction, the absorption peak of I_2 (around 368 nm and in the wide visible light wavelength range) could be clearly seen in the UV-vis spectrum. As reaction time is prolonged (within 2 h), the absorption intensity of iodine is further enhanced (around 292 and 368 nm), while the absorption intensity of ferric (around 430 nm) is reduced (Figure S7). These results verify the reliability of our detection method and support the mechanism.

In addition, by comparing with the spectrum of FeBr_3 or the mixture of $\text{FeBr}_3/\text{EPA-TEMPO}$, the absorption peaks of FeBr_3 (around 270, 358, and 430 nm) are absent in the spectra of

this reaction system (Figure 3d, red line).⁵⁰ By contrast, the absorption peaks of FeBr_3 appear in the spectrum using EBPA as the initiator (Figure 3b,d, black line), even without the addition of TEMPO (Figure S6). These results supported that Fe(III) is difficult to coexist with I^- , as the latter reduces the former to Fe(II) with the generation of I_2 . Further verification of the mechanism was obtained via electron paramagnetic resonance (EPR) spectroscopy. Various Fe(III) complexes, $\text{FeBr}_n\text{I}_m\text{R}_{3-m-n}$, may be detected in the solid state, that is, on flash-frozen solutions of the polymerization systems. A solution of FeBr_2 with EBPA or EIPA (1 equiv) in THF was prepared (Figure 4a). The spectrum of the EBPA system (red line)

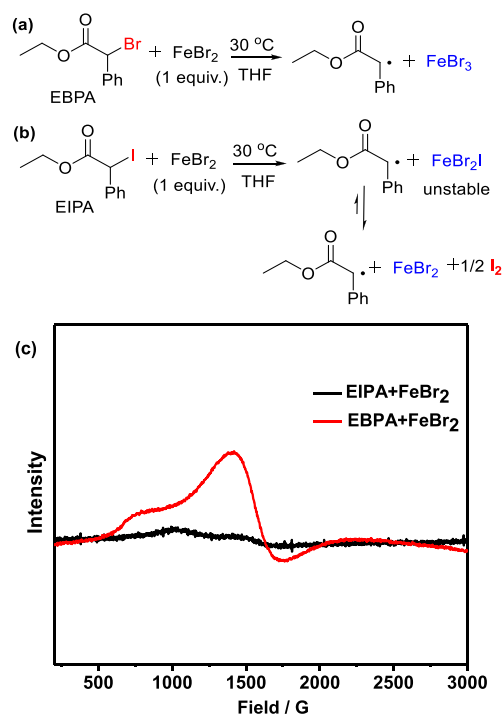
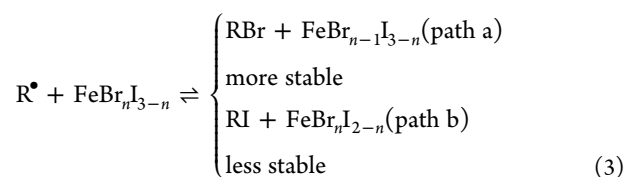


Figure 4. Schemes and EPR spectra (after 12 h) for the reactions of the initiator (32.5 mM) with FeBr_2 (32.5 mM).

shown in Figure 4c was recorded at -170°C , with the signal at $\sim 1500 \text{ G}$ being assigned to Fe(III).¹⁰ The spectrum almost overlaps with that of the FeBr_3 solution in THF (Figure S8). This result is consistent with the normal atom-transfer mechanism. By contrast, as for the spectrum of the EIPA system (Figure 4b), the signal around 1500 G is very feeble (black line), suggesting the instability of I-Fe(III) as I^- could reduce Fe(III) to Fe(II).

I_2 -Mediated Deactivation. As discussed above, I_2 acts as an efficient deactivator (regulator of radical concentration) in our polymerization systems, and excessive I_2 will hinder the polymerization (run 5 in Table 1). Besides, different initiators (EBPA or EIPA) have little effect on the controllability in the presence of I_2 . Furthermore, the polymer obtained with 3/1 ratio of $n(\text{EIPA})/n(\text{FeBr}_3)$ [$n(\text{I})_0/n(\text{Br})_0 = 1/1$] was subjected to elemental analysis (Table S8). In literature,^{1,56–59} in a mixed halide initiating system for traditional ATRP, R-X/Mt-Y (X, Y = Br or Cl), the bulk of the polymer chains is terminated by chlorine because of the stronger alkyl-chloride bond. Accordingly, if $\text{FeBr}_n\text{I}_{3-n}$ (with the I^- from the initiator EIPA during the atom-transfer process) acts as a deactivator (eq 3) via a traditional ATRP process rather than I_2 (eq 1) to

regulate the polymerization, the polymer obtained with 3/1 ratio of $n(\text{EIPA})/n(\text{FeBr}_3)$ ($n(\text{I})_0/n(\text{Br})_0 = 1/1$) should be mostly terminated by bromine (path a) because of the stronger alkyl–bromide bond than alkyl–iodide bond. However, the result shows that in the polymer, the content of iodine is more than 2000 times that of bromine, which suggests the I_2 -mediated deactivation process. Next, we studied the Br–I transformation to further confirm the above conclusion, using R–I (EIPA) with Bu_4NBr ($n_0(\text{I})/n_0(\text{Br}) = 1/1$) as a low mass system in THF-d^8 at room temperature. Figure S9 shows that EIPA is mostly transformed to EBPA (yield $\approx 80\%$) with Bu_4NBr . This reaction is reversible and reaches equilibrium in a short period of time (within 30 min), which confirms that R–Br is more thermodynamically stable than R–I.



Minor Contribution of Degenerative Chain Transfer. Mechanistically, in the polymerization system, degenerative chain transfer (DT) (activation of Polymer-I by Polymer $^\bullet$) should also occur as an activation process. Based on literature,³⁹ the DT constant ($C_{\text{ex}} = 1.6$) for MMA is so small that the DT mechanism alone cannot achieve polydispersity index < 1.7 in batch. The D values of the polymers obtained from our catalytic system are generally around 1.2, suggesting that the contribution of DT to control the polymerization should be minor. Besides, under similar conditions, we conducted the polymerization of MMA using a pure DT system (iodine-transfer polymerization) at 30 °C, which did not include the iron catalyst but employed $\text{Et}_3\text{B}/\text{O}_2$ as the conventional radical initiator (Scheme S2). A very large D value (2.9) is observed with this pure DT system, which clearly indicates that the polydispersity is regulated with only a small contribution from DT in our polymerization system.

CONCLUSIONS

In summary, our side-armed β -ketamine/ $\text{FeBr}_3/\text{Fe}(0)$ catalytic system performs excellently in the controlled radical polymerization and realizes several achievements, which are challengeable for common iron catalytic system. The key to these outstanding achievements lies in the regulation effect of in situ formed I_2 toward radical concentration. The mechanism we proposed is supported by all the experimental results, which involves the ATRP activation process by $\text{Fe}(\text{II})$ and the I_2 -mediated deactivation process. This work provides a new strategy for the design of highly efficient, versatile, green, and robust catalytic system for well-controlled radical polymerizations.

ASSOCIATED CONTENT

Supporting Information

The Supporting Information is available free of charge at <https://pubs.acs.org/doi/10.1021/acscatal.0c04312>.

Experimental procedures, results, and characterizations (PDF)

AUTHOR INFORMATION

Corresponding Authors

Xiao-Yan Wang – State Key Laboratory of Organometallic Chemistry, Shanghai Institute of Organic Chemistry, Chinese Academy of Sciences, Shanghai 200032, China; orcid.org/0000-0002-6367-565X; Email: wangxiaoyan@sioc.ac.cn

Yong Tang – State Key Laboratory of Organometallic Chemistry, Shanghai Institute of Organic Chemistry, Chinese Academy of Sciences, Shanghai 200032, China; orcid.org/0000-0002-5435-9938; Email: tangy@sioc.ac.cn

Authors

Zhi-Hao Chen – State Key Laboratory of Organometallic Chemistry, Shanghai Institute of Organic Chemistry, Chinese Academy of Sciences, Shanghai 200032, China; School of Physical Science and Technology, ShanghaiTech University, Shanghai 201210, China; University of Chinese Academy of Sciences, Beijing 100049, China

Yang Ma – State Key Laboratory of Organometallic Chemistry, Shanghai Institute of Organic Chemistry, Chinese Academy of Sciences, Shanghai 200032, China; School of Physical Science and Technology, ShanghaiTech University, Shanghai 201210, China; University of Chinese Academy of Sciences, Beijing 100049, China

Xiu-Li Sun – State Key Laboratory of Organometallic Chemistry, Shanghai Institute of Organic Chemistry, Chinese Academy of Sciences, Shanghai 200032, China

Jun-Fang Li – State Key Laboratory of Organometallic Chemistry, Shanghai Institute of Organic Chemistry, Chinese Academy of Sciences, Shanghai 200032, China

Ben-Hu Zhu – State Key Laboratory of Organometallic Chemistry, Shanghai Institute of Organic Chemistry, Chinese Academy of Sciences, Shanghai 200032, China

Complete contact information is available at: <https://pubs.acs.org/10.1021/acscatal.0c04312>

Author Contributions

This manuscript was written through contributions of all authors. All authors have given approval to the final version of the manuscript.

Notes

The authors declare no competing financial interest.

ACKNOWLEDGMENTS

This study was dedicated to the Southern University of Science and Technology on the occasion of its 10th anniversary. The authors are grateful for the financial support by Youth Innovation Promotion Association CAS (no. 2020259), Shanghai Sailing Program (18YF1429000), and the National Natural Science Foundation of China (21901253, 21690072, and 21672237).

REFERENCES

- (1) Matyjaszewski, K.; Xia, J. Atom Transfer Radical Polymerization. *Chem. Rev.* **2001**, *101*, 2921–2990.
- (2) Kamigaito, M.; Ando, T.; Sawamoto, M. Metal-Catalyzed Living Radical Polymerization. *Chem. Rev.* **2001**, *101*, 3689–3746.
- (3) Hu, R.; Leung, N. L. C.; Tang, B. Z. AIE macromolecules: syntheses, structures and functionalities. *Chem. Soc. Rev.* **2014**, *43*, 4494–4562.
- (4) Li, B.; Yu, B.; Ye, Q.; Zhou, F. Tapping the Potential of Polymer Brushes through Synthesis. *Acc. Chem. Res.* **2015**, *48*, 229–237.

- (5) Ouchi, M.; Terashima, T.; Sawamoto, M. Transition Metal-Catalyzed Living Radical Polymerization: Toward Perfection in Catalysis and Precision Polymer Synthesis. *Chem. Rev.* **2009**, *109*, 4963–5050.
- (6) di Lena, F.; Matyjaszewski, K. Transition metal catalysts for controlled radical polymerization. *Prog. Polym. Sci.* **2010**, *35*, 959–1021.
- (7) Matyjaszewski, K.; Tsarevsky, N. V. Nanostructured functional materials prepared by atom transfer radical polymerization. *Nat. Chem.* **2009**, *1*, 276–288.
- (8) O'Reilly, R. K.; Gibson, V. C.; White, A. J. P.; Williams, D. J. Design of Highly Active Iron-Based Catalysts for Atom Transfer Radical Polymerization: Tridentate Salicylaldiminato Ligands Affording near Ideal Nernstian Behavior. *J. Am. Chem. Soc.* **2003**, *125*, 8450–8451.
- (9) Whitfield, R.; Anastasaki, A.; Nikolaou, V.; Jones, G. R.; Engels, N. G.; Discekici, E. H.; Fleischmann, C.; Willenbacher, J.; Hawker, C. J.; Haddleton, D. M. Universal Conditions for the Controlled Polymerization of Acrylates, Methacrylates, and Styrene via Cu(0)-RDRP. *J. Am. Chem. Soc.* **2017**, *139*, 1003–1010.
- (10) Schroeder, H.; Lake, B. R. M.; Demeshko, S.; Shaver, M. P.; Buback, M. A Synthetic and multispectroscopic speciation analysis of controlled radical polymerization mediated by amine–bis(phenolate) iron complexes. *Macromolecules* **2015**, *48*, 4329–4338.
- (11) Simakova, A.; Mackenzie, M.; Averick, S. E.; Park, S.; Matyjaszewski, K. Bioinspired iron-based catalyst for atom transfer radical polymerization. *Angew. Chem., Int. Ed.* **2013**, *52*, 12148–12151.
- (12) Mohammad Rabea, A.; Zhu, S. Controlled radical polymerization at high conversion: Bulk ICAR ATRP of methyl methacrylate. *Ind. Eng. Chem. Res.* **2014**, *53*, 3472–3477.
- (13) Ding, M.; Jiang, X.; Peng, J.; Zhang, L.; Cheng, Z.; Zhu, X. An atom transfer radical polymerization system: Catalyzed by an iron catalyst in PEG-400. *Green Chem.* **2015**, *17*, 271–278.
- (14) Xue, Z.; Linh, N. T. B.; Noh, S. K.; Lyoo, W. S. Phosphorus-Containing Ligands for Iron(III)-Catalyzed Atom Transfer Radical Polymerization. *Angew. Chem., Int. Ed.* **2008**, *47*, 6426–6429.
- (15) Kotani, Y.; Kamigaito, M.; Sawamoto, M. $\text{FeCp}(\text{CO})_2\text{I}$: A Phosphine-Free Half-Metallocene-Type Iron(II) Catalyst for Living Radical Polymerization of Styrene. *Macromolecules* **1999**, *32*, 6877–6880.
- (16) Niibayashi, S.; Hayakawa, H.; Jin, R.-H.; Nagashima, H. Reusable and environmentally friendly ionic trinuclear iron complex catalyst for atom transfer radical polymerization. *Chem. Commun.* **2007**, 1855–1857.
- (17) Gibson, V. C.; O'Reilly, R. K.; Reed, W.; Wass, D. F.; White, A. J. P.; Williams, D. J. Four-coordinate iron complexes bearing α -diimine ligands: efficient catalysts for Atom Transfer Radical Polymerization (ATRP). *Chem. Commun.* **2002**, 1850–1851.
- (18) Louie, J.; Grubbs, R. H. Highly active iron imidazolyidene catalysts for atom transfer radical polymerization. *Chem. Commun.* **2000**, 1479–1480.
- (19) Zhu, S.; Yan, D. Atom Transfer Radical Polymerization of Methyl Methacrylate Catalyzed by Iron^{II} Chloride/Isophthalic Acid System. *Macromolecules* **2000**, *33*, 8233–8238.
- (20) Ishio, M.; Katsube, M.; Ouchi, M.; Sawamoto, M.; Inoue, Y. Active, Versatile, and Removable Iron Catalysts with Phosphazanium Salts for Living Radical Polymerization of Methacrylates. *Macromolecules* **2009**, *42*, 188–193.
- (21) Sarbu, T.; Matyjaszewski, K. ATRP of Methyl Methacrylate in the Presence of Ionic Liquids with Ferrous and Cuprous Anions. *Macromol. Chem. Phys.* **2001**, *202*, 3379–3391.
- (22) Wang, Y.; Matyjaszewski, K. ATRP of MMA Catalyzed by $\text{Fe}^{\text{II}}\text{Br}_2$ in the Presence of Triflate Anions. *Macromolecules* **2011**, *44*, 1226–1228.
- (23) Bian, C.; Zhou, Y.-N.; Guo, J.-K.; Luo, Z.-H. Visible-Light-Induced Atom-Transfer-Radical Polymerization with a ppm-Level Iron Catalyst. *Ind. Eng. Chem. Res.* **2017**, *56*, 4949–4956.
- (24) Okada, S.; Park, S.; Matyjaszewski, K. Initiators for Continuous Activator Regeneration Atom Transfer Radical Polymerization of Methyl Methacrylate and Styrene with N-Heterocyclic Carbene as Ligands for Fe-Based Catalysts. *ACS Macro Lett.* **2014**, *3*, 944–947.
- (25) Mukumoto, K.; Wang, Y.; Matyjaszewski, K. Iron-Based ICAR ATRP of Styrene with ppm Amounts of $\text{Fe}^{\text{III}}\text{Br}_3$ and 1,1'-Azobis(cyclohexanecarbonitrile). *ACS Macro Lett.* **2012**, *1*, 599–602.
- (26) Nishizawa, K.; Ouchi, M.; Sawamoto, M. Phosphine–Ligand Decoration toward Active and Robust Iron Catalysts in LRP. *Macromolecules* **2013**, *46*, 3342–3349.
- (27) He, W.; Zhang, L.; Miao, J.; Cheng, Z.; Zhu, X. Facile Iron-Mediated AGET ATRP for Water-Soluble Poly(ethylene glycol) Monomethyl Ether Methacrylate in Water. *Macromol. Rapid Commun.* **2012**, *33*, 1067–1073.
- (28) Fujimura, K.; Ouchi, M.; Sawamoto, M. Ferrocene Cocatalysis for Iron-Catalyzed Living Radical Polymerization: Active, Robust, and Sustainable System under Concerted Catalysis by Two Iron Complexes. *Macromolecules* **2015**, *48*, 4294–4300.
- (29) Dadashi-Silab, S.; Matyjaszewski, K. Iron Catalysts in Atom Transfer Radical Polymerization. *Molecules* **2020**, *25*, 1648.
- (30) O'Reilly, R. K.; Shaver, M. P.; Gibson, V. C.; White, A. J. P. α -Diimine, Diamine, and Diphosphine Iron Catalysts for the Controlled Radical Polymerization of Styrene and Acrylate Monomers. *Macromolecules* **2007**, *40*, 7441–7452.
- (31) Ishio, M.; Terashima, T.; Ouchi, M.; Sawamoto, M. Carbonyl–Phosphine Heteroligation for Pentamethylcyclopentadienyl (Cp^*)–Iron Complexes: Highly Active and Versatile Catalysts for Living Radical Polymerization. *Macromolecules* **2010**, *43*, 920–926.
- (32) Rolland, M.; Truong, N. P.; Whitfield, R.; Anastasaki, A. Tailoring Polymer Dispersity in Photoinduced Iron-Catalyzed ATRP. *ACS Macro Lett.* **2020**, *9*, 459–463.
- (33) Dadashi-Silab, S.; Matyjaszewski, K. Iron-Catalyzed Atom Transfer Radical Polymerization of Semifluorinated Methacrylates. *ACS Macro Lett.* **2019**, *8*, 1110–1114.
- (34) Dadashi-Silab, S.; Pan, X.; Matyjaszewski, K. Photoinduced Iron-Catalyzed Atom Transfer Radical Polymerization with ppm Levels of Iron Catalyst under Blue Light Irradiation. *Macromolecules* **2017**, *50*, 7967–7977.
- (35) Ni, Y.; Zhang, L.; Cheng, Z.; Zhu, X. Iodine-mediated reversible-deactivation radical polymerization: a powerful strategy for polymer synthesis. *Polym. Chem.* **2019**, *10*, 2504–2515.
- (36) Matyjaszewski, K.; Gaynor, S.; Wang, J.-S. Controlled Radical Polymerizations: The Use of Alkyl Iodides in Degenerative Transfer. *Macromolecules* **1995**, *28*, 2093–2095.
- (37) Lacroix-Desmazes, P.; Severac, R.; Boutevin, B. Reverse Iodine Transfer Polymerization of Methyl Acrylate and n-Butyl Acrylate. *Macromolecules* **2005**, *38*, 6299–6309.
- (38) Goto, A.; Zushi, H.; Hirai, N.; Wakada, T.; Tsujii, Y.; Fukuda, T. Living Radical Polymerizations with Germanium, Tin, and Phosphorus Catalysts—Reversible Chain Transfer Catalyzed Polymerizations (RTCPs). *J. Am. Chem. Soc.* **2007**, *129*, 13347–13354.
- (39) Goto, A.; Ohtsuki, A.; Ohfujii, H.; Tanishima, M.; Kaji, H. Reversible Generation of a Carbon-Centered Radical from Alkyl Iodide Using Organic Salts and Their Application as Organic Catalysts in Living Radical Polymerization. *J. Am. Chem. Soc.* **2013**, *135*, 11131–11139.
- (40) Tian, C.; Wang, P.; Ni, Y.; Zhang, L.; Cheng, Z.; Zhu, X. A Facile Photocontrolled Iodine-Mediated Reversible-Deactivation Radical Polymerization System: Solution Polymerization of Methacrylates under Irradiation with NIR LED Light. *Angew. Chem., Int. Ed.* **2019**, *59*, 3910–3916.
- (41) Yang, H.; Wang, Z.; Zheng, Y.; Huang, W.; Xue, X.; Jiang, B. Synthesis of highly branched polymers by reversible complexation-mediated copolymerization of vinyl and divinyl monomers. *Polym. Chem.* **2017**, *8*, 2137–2144.
- (42) David, G.; Boyer, C.; Tonnar, J.; Ameduri, B.; Lacroix-Desmazes, P.; Boutevin, B. Use of Iodocompounds in Radical Polymerization. *Chem. Rev.* **2006**, *106*, 3936–3962.

(43) Liao, S.; Sun, X.-L.; Tang, Y. Side Arm Strategy for Catalyst Design: Modifying Bisoxazolines for Remote Control of Enantioselectivity and Related. *Acc. Chem. Res.* **2014**, *47*, 2260–2272.

(44) Wang, X.-Y.; Sun, X.-L.; Wang, F.; Tang, Y. SaBOX/Copper Catalysts for Highly Syndio-Specific Atom Transfer Radical Polymerization of Methyl Methacrylate. *ACS Catal.* **2017**, *7*, 4692–4696.

(45) Schaubach, S.; Wang, X.-Y.; Li, J.-F.; Sun, X.-L.; Wang, S. R.; Tang, Y. Yb(N Tf₂)₃/HFIP induced high isotacticity in atom transfer radical polymerization of methyl methacrylate. *Polym. Chem.* **2018**, *9*, 4711–4715.

(46) Wang, X.-Y.; Sun, X.-L.; Chen, Z.-H.; Wang, F.; Wang, S. R.; Tang, Y. Highly efficient access to well-defined linear polymers with substantial vinyl pendants via ATRP of divinyl monomers. *Polym. Chem.* **2018**, *9*, 4309–4315.

(47) Wang, X.-Y.; Chen, Z.-H.; Sun, X.-L.; Tang, Y. Low Temperature Effect on ATRP of Styrene and Substituted Styrenes Enabled by SaBOX Ligand. *Polymer* **2019**, *178*, 121630.

(48) Chen, Z.-H.; Wang, X.-Y.; Sun, X.-L.; Li, J.-F.; Zhu, B.-H.; Tang, Y. Highly Efficient Atom Transfer Radical Polymerization System Based on the SaBOX/Copper Catalyst. *Macromolecules* **2019**, *52*, 9792–9798.

(49) Nikolaychuk, P. A.; Kuvaeva, A. O. Studying Equilibrium in the Chemical Reaction between Ferric and Iodide Ions in Solution Using a Simple and Inexpensive Approach. *J. Chem. Educ.* **2016**, *93*, 1267–1269.

(50) Yoon, K. B.; Kochi, J. K. Ferric Iodide as a Nonexistent Compound. *Inorg. Chem.* **1990**, *29*, 869–874.

(51) Kotani, Y.; Kamigaito, M.; Sawamoto, M. FeCp(CO)₂I: A Phosphine-Free Half-Metallocene-Type Iron(II) Catalyst for Living Radical Polymerization of Styrene. *Macromolecules* **1999**, *32*, 6877–6880.

(52) Iodinated initiator is observed to achieve better controllability than its brominated analogue in the living free radical polymerization catalyzed by half-metallocene-type Fe(II) (FeCp(CO)₂I). Kotani, Y.; Kamigaito, M.; Sawamoto, M. Living Radical Polymerization of Styrene by Half-Metallocene Iron Carbonyl Complexes. *Macromolecules* **2000**, *33*, 3543–3549.

(53) Guo, B.; Hou, L.; Li, Y.; Xiao, L. Organocatalyzed controlled radical polymerization with alkyl bromide initiator via in situ halogen exchange under thermal condition. *Polymer* **2020**, *189*, 122201.

(54) Wang, Y.-a.; Shi, Y.; Fu, Z.; Yang, W. Hexamethylphosphoramide as a highly reactive catalyst for the reversible-deactivation radical polymerization of MMA with an in situ formed alkyl iodide initiator. *Polym. Chem.* **2017**, *8*, 6073–6085.

(55) Liu, X.; Xu, Q.; Zhang, L.; Cheng, Z.; Zhu, X. Visible-light-induced living radical polymerization using in situ bromine-iodine transformation as an internal boost. *Polym. Chem.* **2017**, *8*, 2538–2551.

(56) Khouba, Z.; Benabdallah, T.; Maschke, U. Spectrophotometric investigation of interaction between iodine and pentadentate Schiff base ligands. *Spectrochim. Acta, Part A* **2014**, *125*, 61–66.

(57) Shipp, D. A.; Wang, J.-L.; Matyjaszewski, K. Synthesis of Acrylate and Methacrylate Block Copolymers Using Atom Transfer Radical Polymerization. *Macromolecules* **1998**, *31*, 8005–8008.

(58) Matyjaszewski, K.; Shipp, D. A.; Wang, J.-L.; Grimaud, T.; Patten, T. E. Utilizing Halide Exchange To Improve Control of Atom Transfer Radical Polymerization. *Macromolecules* **1998**, *31*, 6836–6840.

(59) Ando, T.; Kamigaito, M.; Sawamoto, M. Reversible Activation of Carbon-Halogen Bonds by RuCl₂(PPh₃)₃: Halogen Exchange Reactions in Living Radical Polymerization. *Macromolecules* **2000**, *33*, 2819–2824.